Bulletin of the Seismological Society of America, Vol. 77, No. 6, pp. 1984–2004, December 1987

SOURCE MECHANISM OF THE MAGNITUDE 7.2 GRAND BANKS EARTHQUAKE OF NOVEMBER 1929: DOUBLE COUPLE OR SUBMARINE LANDSLIDE?

BY H. S. HASEGAWA AND H. KANAMORI

ABSTRACT

We have examined *P*, *S*, and surface waves derived from seismograms that we collected for the 1929 Grand Banks, Canada, earthquake. This event is noteworthy for the sediment slide and turbidity current that broke the trans-Atlantic cables and for its destructive tsunami. Both the surface-wave magnitude, M_S, and the body-wave magnitude, m_B, calculated from these seismograms are 7.2. Fault mechanisms previously suggested for this event include a NW-SE-striking strike-slip mechanism and an approximately E-W-striking thrust mechanism. In addition, because of the presence of an extensive area of slump and turbidity current, there exists the possibility that sediment slumping could also be a primary causative factor of this event. We tested these fault models and a horizontal single-force (oriented N5°W) model representing a sediment slide against our data. Among these models, only the single-force model is consistent with the *P*-, *S*-, and surface-wave data. Our data, however, do not preclude fault models which were not tested. From the spectral data of Love waves at a 50-sec period, we estimated the magnitude of the single force to be about 1.4×10^{20} dynes. From this value, we estimated the total volume of sedimentary slumping to be about 5.5×10^{11} m^3, which is approximately 5 times larger than a recent estimate of volume from *in situ* measurements. The difference in estimates of overall volume is likely due to a combination of the inherent difficulty in estimating accurately the displaced sediments from *in situ* measurements, and of inadequacy of the seismic model; or perhaps because not only the slump but also a tectonic earthquake could have been the cause of this event and contributed significantly to the waveforms studied.

INTRODUCTION

The M_S 7.2 "Grand Banks" earthquake of 1929 is noteworthy not only because of its size (largest historical earthquake in Atlantic Canada), but also because of its connection with both a tsunami and a turbidity current. The destructive tsunami caused the loss of 27 lives and extensive property damage to dwellings and fishing equipment along Burin Peninsula of southern Newfoundland (Doxsee, 1948), located approximately 250 km north of the epicenter (see Figure 1). In the epicentral region, a submarine landslide transformed into a turbidity current (Heezen and Ewing, 1952), which flowed as far as 1,700 km and ruptured trans-Atlantic cables in 28 places (Doxsee, 1948). More than 5×10^{10} m^3 of sediments slumped down the continental slope, with lateral extent of slumping extending possibly out to about 250 km along the continental margin (see Piper and Normark, 1982; Piper *et al.*, 1985b).

A rather intriguing aspect of the 1929 earthquake, for which the epicenter is near the top of the continental slope, is the suggestion (e.g., see Gussow, 1982) that the actual source mechanism could be submarine slumping *per se*. Examples of seismic events related to a slump mechanism are the combined landslide-eruption at Mount St. Helens (Kanamori and Given, 1982) and large-scale gravitational sliding down the southern flank of the Kilauea volcano in 1975 (Ando, 1979; Furumoto and

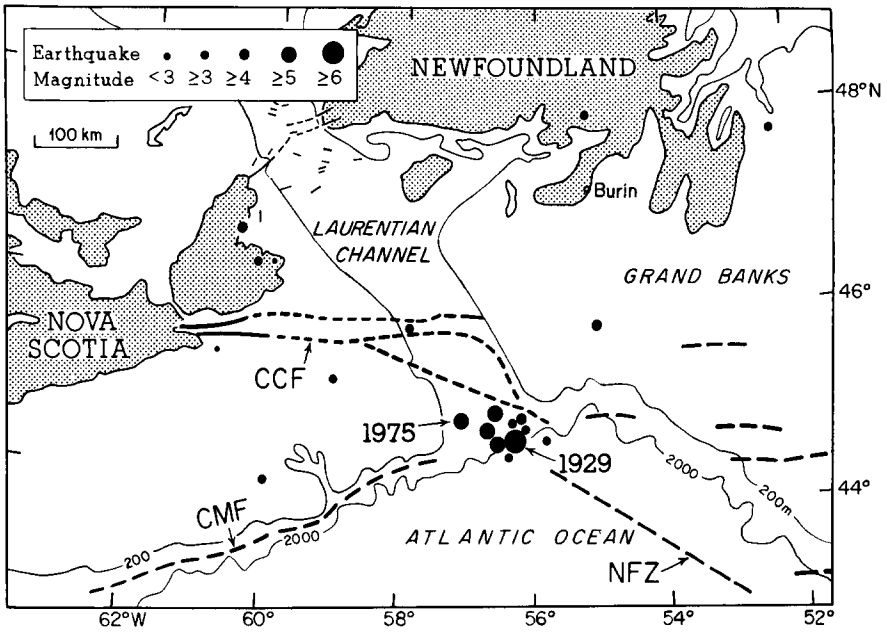

FIG. 1. Epicenters of maritime Atlantic Canada earthquakes from 1929 to 1980. Bathymetry contours are in meters. Offshore basement faults are drawn as continuous curves when certain and dashed line segments when uncertain. 1929 = Grand Banks earthquake of 1929; 1975 = Laurentian Channel earthquake of 1975; CCF = Cobequid-Chedabucto fault; CMF = (hypothesized) Continental Margin Faults of type described by Turcotte *et al.* (1977); NFZ = westerly extension of Newfoundland Fracture Zone (cf. Fletcher *et al.*, 1978). (After Basham *et al.*, 1983.)

Kovach, 1979; Nakamura, 1980; Crosson and Endo, 1981, 1982; Eissler and Kanamori, 1987). Analysis of long-period surface waves generated by the Mount St. Helens landslide eruption in 1980 indicates that a single, approximately horizontal force of 10^{18} dynes directed opposite to the landslide can account for the observed two-lobed radiation pattern of long-period Love waves (Kanamori and Given, 1982). Long-period surface waves from the M_S 7.2 Kalapana, Hawaii, earthquake can be modeled by a single (shallow dipping) force of approximately 10^{20} dynes (Eissler and Kanamori, 1987). *P*-wave first motions of the 1946 Aleutian Island event (see Kanamori, 1972) can also be interpreted in terms of a single force source mechanism (Kanamori, 1985). In this paper, we investigate whether or not submarine slumping *per se* as a source mechanism can account for observed seismic waveforms and, if so, the strength and duration of the associated single force and the volume of (unstable) sediments that experienced "instantaneous" slumping.

With commencement for hydrocarbon exploration along the continental margin of Atlantic Canada, a proper understanding of the seismotectonics, especially as it relates to seismic risk of both onshore and offshore facilities, is becoming more imperative (see Basham *et al.*, 1983; Page and Basham, 1985). Of particular relevance are the duration and frequency content of strong ground motion, the liquefaction potential, and the tsunamigenic potential of larger offshore seismic events.

SEISMICITY AND SEISMOTECTONICS

Figure 1 shows known seismicity in the epicentral region of the 1929 Grand Banks earthquake. A revised epicenter for the 1929 Grand Banks earthquake of 18 November, with onset time of 20h 32m 00s, is 44.69°N, 56.00°W (Dewey and Gordon, 1984). The only other earthquake in this cluster that has been analyzed in

detail is the M 5.2 Laurentian Channel earthquake of 1975; for this event, Hasegawa and Herrmann (in preparation) have obtained a focal depth of 30 ± 3 km (in the upper mantle) and a predominantly thrust source mechanism, with the deviatoric compression vector subhorizontal and in the NE-SW quadrant. *In situ* stress measurements in boreholes on the continental margin near the earthquake cluster also indicate minimum (deviatoric) extension in a NW-SE direction and hence maximum (compressive) principal stress in an approximately NE-SW direction (Podrouzek and Bell, 1985).

Although active faults have not been positively identified near the cluster of earthquakes at the mouth of the Laurentian Channel, it has been hypothesized that the 1929 event may have occurred along a landward extension of the Newfoundland Fracture Zone (a transform plate boundary) (Fletcher *et al.*, 1978), along (originally normal) faults that exist along passive continental margins due to sediment loading (Turcotte *et al.*, 1977), or along strike-slip faults (Stewart, 1979). Furthermore, J. Adams (personal communication, 1985) suggests that epicenters of the earthquake cluster near the mouth of the Laurentian Channel appear to be confined to a rectangular box of about 100 km by 35 km, which could be an indication of a common plane of failure associated with the 1929 event (see Figure 1). Thus, in all, three different (strike-slip, dip-slip and slump) types of source mechanisms have been postulated for the 1929 event.

Data Base

We have collected records of this noteworthy historical earthquake from approximately 50 seismograph stations distributed around the world. This data base has been acquired over a number of years from many different sources: microfilms and historical records in Ottawa; microfilms based on the listing by Glover and Meyers (1982) at the World Data Center A at Boulder and at the World Data Center B in Moscow; copies from the St. Louis University network; and copies from a number of seismograph stations that reported this event to the International Seismological Summary.

Magnitude

Magnitude calculations of the 1929 Grand Banks earthquake are listed in Table 1 and indicate average magnitude values of M_S = 7.2 and m_B 7.2. These values are in agreement with the estimates by Gutenberg and Richter (1956) and Dewey and Gordon (1984).

P-Wave First Motions

A careful scrutiny of the collection of records indicates 14 stations are useful for determining P-wave first motions. Table 2 lists these records as well as the procedure and criteria used to determine the sense and reliability of P-wave first motion. Unfortunately, the wide disparity in instrument response and in recording and annotation precludes the use of many of the other collected records for P-wave first motion studies. In addition, the presence of the Atlantic Ocean prevents good azimuthal coverage east of the epicenter. The first-motion data plotted on an equal-area projection of the lower focal hemisphere are shown in Figure 2.

S-Wave Polarity

The S waves were clearly recorded by Galitzin seismographs at UCCLE and KEW (Figure 3). At these stations, the S waves are almost naturally rotated into

TABLE 1

MAGNITUDE CALCULATION OF THE 1929 GRAND BANKS EARTHQUAKE

Station	Epicentral Distance (°)	Body-Wave Component*	m_B	Surface-Wave Component†	M_S
Copenhagen	43.5	*S*	7.2	*RH*	7.1
EBRO	40.9	*S*	6.9		
Granada	39.7	*PH*	7.3	*RH*	7.2
		S	7.3		
Graz	48.2	*PH*	7.3	*RH*	7.6
		S	7.0		
Heligoland	41.3	*S*	7.0	*RH*	7.2
Helwan	67.9	*PH*	7.4	*RH*	7.1
		S	7.4		
KEW	37.1	*S*	7.0		
La Paz	61.7	*PH*	7.5	*RH*	7.1
		S	7.0		
Potsdam	44.8	*S*	7.2	*RH*	6.9
Rio de Janeiro	68.0	*PH*	7.2	*RH*	7.2
		S	7.3		
Stonyhurst	35.4	*PH*	7.0	*RH*	7.1
Tucson	44.0	*PH*	6.9	*RH*	7.3
UCCLE	40.1	*S*	7.1		
		Mean value of $m_B = 7.2 \pm 0.2$		Mean $M_S = 7.2 \pm 0.2$	

* *PH* = horizontal component of *P* wave and *S* = *SH* wave (short- and long-period).
† *RH* = radial component of fundamental Rayleigh wave (20-sec period).

SH and *SV* components. The N-S and E-W components correspond to almost *SH* and *SV*, respectively. The initial motion on the N-S component (*SH*) is sharp and toward north at both UCCLE and KEW. The initial motion of the E-W component at UCCLE is slightly smaller than the N-S component. It is distinct and toward west. The initial motion of the E-W component at KEW is somewhat ambiguous, but is probably toward west. The vertical arrows are positioned at the apparent onset of the N-S (*SH*) component. However, because of "noise" preceding this phase, the actual onset could be a few seconds earlier, which would agree with the onset of the E-W (*SV*) component. The consistency of the *S*-wave polarity at two stations with the same azimuth from the epicenter would argue against any of these records having incorrect (N-S or E-W) direction labels. The first motion of the *SV* component at both stations is followed by large phases which are probably *S*-coupled *PL* waves. Table 3 summarizes the result.

The response of the N-S (*N*) and corresponding E-W (*E*) component of the Galitzin seismographs at both UCCLE and KEW are remarkably well-matched and, therefore, phase lags between (*N*) and (*E*) components are negligible. For example, at UCCLE the instrument parameters are as follows: undamped pendulum period (T) is 24.8 sec (*N*) and 24.6 sec (*E*); undamped galvanometer period (T_1) is 24.5 sec (*N*) and 24.5 sec (*E*); distance between galvanometer and drum (A) is 103.4 cm (*N*) and 103.7 cm (E); damping constant (μ^2) is 0.03 (*N*) and −0.01 (E); transmission

TABLE 2

DATA FOR *P*-WAVE FIRST MOTIONS

Station	Distance (°)	Azimuth to Station (°)	Back Azimuth (°)	Vertical* (*U*, *D*)	N-S	E-W	Description of First Motion
Ann Arbor	20.3	273	74.3	—	—	*eP*(*E*)	Therefore inferred to be down (*D*)
Buffalo	16.7	273	76.7	—	—	*eP*(*W*)	Therefore inferred to be up (*C*)
Copenhagen	43.5	50	285.0	*iP*(*U*)	—	*eP*(*E*)	Therefore up (*C*)
EBRO	40.9	75	294.0	—	*eP*(*S*)	*eP*(*E*)	Therefore probably up (*C*)
Granada	39.7	82	297.0	*iP*(*U*)	—	*eP*(*W*)	Ambiguous, but *iP*(*U*) distinct; therefore probably up (*C*)
KEW	37.1	59	282.0	*eP*(*U*)	—	*eP*(*E*)	Therefore up (*C*)
La Paz	61.7	193	9.9	*eP*(*D*)	*eP*(*N*)	—	Therefore down (*D*)
St. Louis	26.2	269	66.0	—	—	*eP*(*W*)	Therefore inferred to be up (*C*)
Stonyhurst	35.4	55	277.0	—	—	*eP*(*E*)	Therefore inferred to be up (*C*)
Toronto	16.9	275	79.0	—	*eP*(*S*)	*iP*(*W*)	Therefore probably up (*C*)
UCCLE	40.1	59	285.0	*eP*(*U*)	*eP*(*S*)	*iP*(*E*)	Therefore up (*C*)
Potsdam	44.8	54	289.0	—	*eP*(*S*)	*iP*(*E*)	Ambiguous, but *eP*(*S*) before *iP*(*W*); therefore inferred to be up (*C*)
Tucson	44.0	273	57.5	—	—	*eP*(*E*)	Therefore inferred to be up (*C*)
Uppsala	45.1	43	284.0	—	*eP*(*N*)	*iP*(*E*)	Therefore probably up (*C*)

* *iP* = impulsive compressional phase; *eP* = emergent compressional phase.

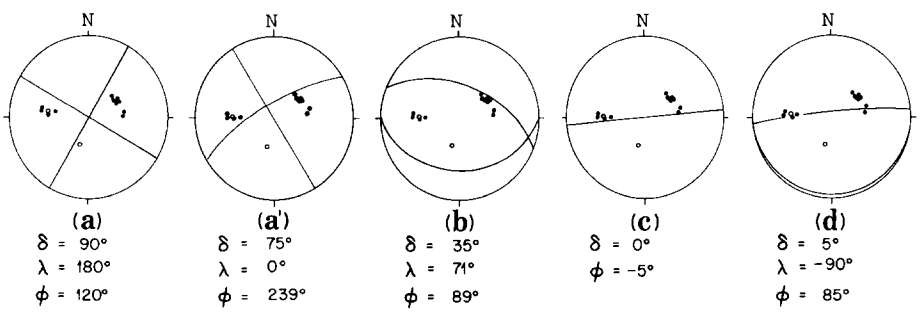

FIG. 2. *P*-wave first-motion data and possible mechanisms. Stereographic projection of lower focal hemisphere is shown. Closed and open symbols denote compressional and dilatational first motions, respectively. (a) Vertical strike-slip; (a′) dipping strike-slip; (b) thrust; (c) single-force; and (d) normal. Symbols δ, λ, and ϕ represent dip, rake, and fault strike, respectively. For single-force mechanism, δ and ϕ are plunge and strike of force, respectively.

factor (K) is 42.1 (N) and 40.3 (E); and clock correction is −7.2 sec (N) and −7.2 sec (E). The corresponding components for KEW are equally well-matched.

These S waves are important to discriminate different mechanisms. Unfortunately, the records from other stations are not clear enough for such detailed analysis.

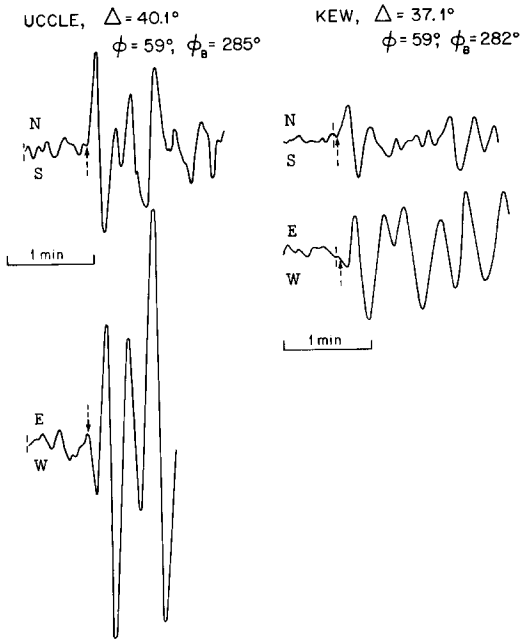

FIG. 3. *S* waves recorded by Galitzin seismographs at UCCLE and KEW. Vertical dashed arrows indicate onset of *S* waves. Short vertical line segment crossing trace before (to *left* of) vertical arrow indicates start of minute mark preceding onset of *S* wave. Clock correction for both N-S and E-W components at UCCLE is −7.2 sec, and at KEW, +12.2 sec.

TABLE 3

DIRECTION OF *S* WAVE AT UCCLE AND KEW*

Mechanism	N-S	E-W
Strike-slip	*S*	*W*
Strike-slip (dipping)	*S*	*E*
Thrust	*S*	*E*
Single-force	*N*	*W*
Normal	*N*	*W*
Observed	*N*	*W*

* Corresponding *P*-nodal planes in Figure 2.

SURFACE-WAVE SPECTRA

Surface-wave analysis to calculate source strength is restricted to records of electromagnetic (Galitzin) seismographs at KEW and UCCLE because mechanical seismographs have insufficient gain in the required period range (40 sec or longer) for a magnitude ~7 earthquake. Surface waves with period near 20 sec are conspicuous on many records and are used to determine M_S. The results are shown in Figure 4 (a and b). An important observation is that at the period of 50 sec where the signal-to-noise ratio is high, the amplitude of the Love wave is much larger than that for the Rayleigh wave. The absence of long-period energy in the Rayleigh wave train is clear in Figure 4 and suggests that both UCCLE and KEW are located close to a radiation node of long-period Rayleigh waves. This feature is obvious in the time-domain records as well.

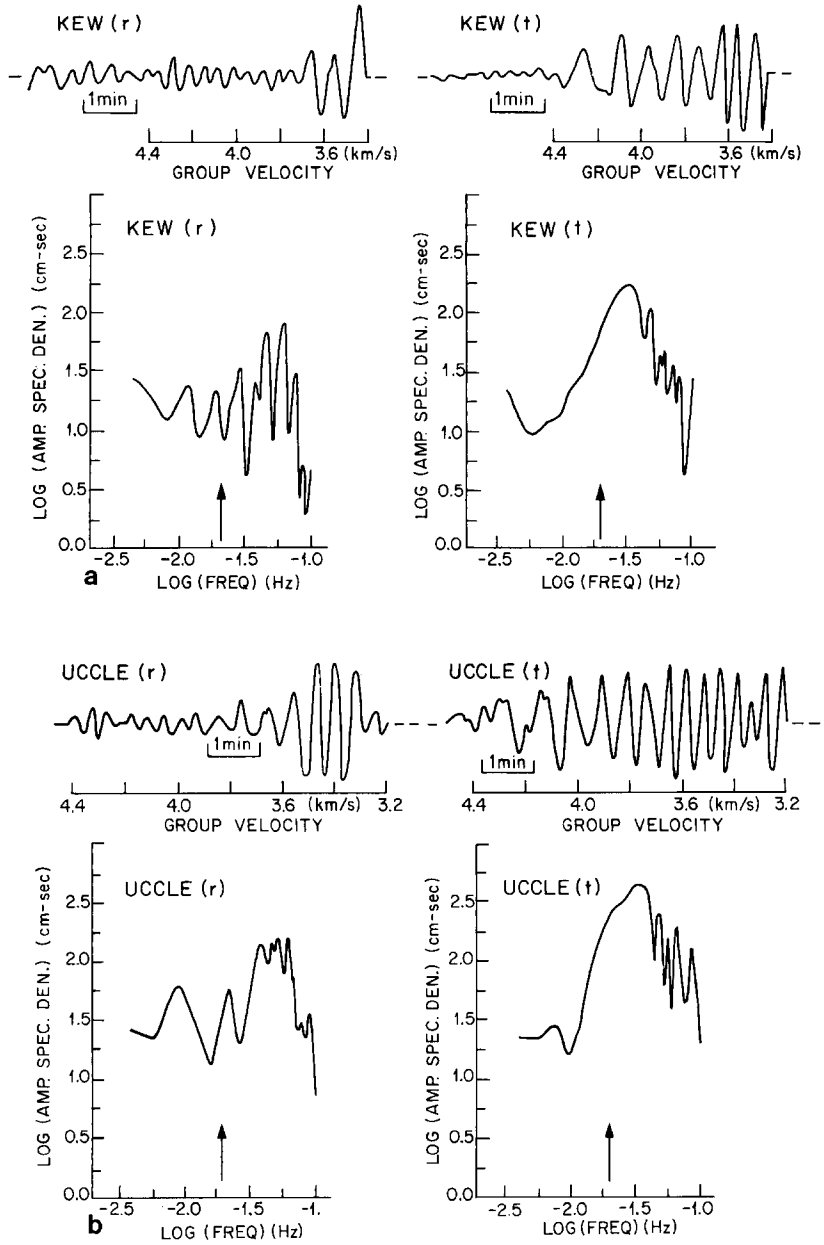

FIG. 4. (a) (*Top trace*) KEW records of fundamental-mode Rayleigh [radial (r)] component and Love [transverse (t)] component. (*Bottom trace*) Corresponding amplitude spectral density. Vertical arrow points to spectral amplitude at log (frequency) = −1.70 (0.02 Hz or 50-sec period). (b) Same as for (a), but for UCCLE records.

INTERPRETATION

The data set presented previously is too incomplete to determine the source mechanism. We therefore test several proposed mechanisms against the data.

Strike-slip mechanism. The first-motion data shown in Figure 2 can be interpreted by a strike-slip mechanism (Figure 2a) similar to the one suggested by

Stewart (1979). However, the direction of *SH* waves at UCCLE and KEW predicted by this model is toward the south, which is opposite the observed direction (Table 3).

The *P*-wave first-motion data constrict the allowable range of the vertical strike-slip planes to a counterclockwise and clockwise rotations of no more than 8° and 10°, respectively.

The amplitude spectra of Love and Rayleigh waves at a 50-sec period computed by the Ben-Menahem *et al.* (1970) method for this strike-slip mechanism are shown in Figure 5a as a function of the azimuth. At the azimuth of UCCLE and KEW (59° from north), this mechanism predicts a larger Rayleigh wave than Love wave, which is contrary to the observation.

However, if one of the nodal planes is allowed to deviate from the vertical, we can find strike-slip mechanisms which can explain the observed Love- to Rayleigh-wave amplitude ratio. For example, a strike-slip mechanism with a strike of 239° and a dip of 75° as shown in Figure 2a′, can explain the observed first-motion data

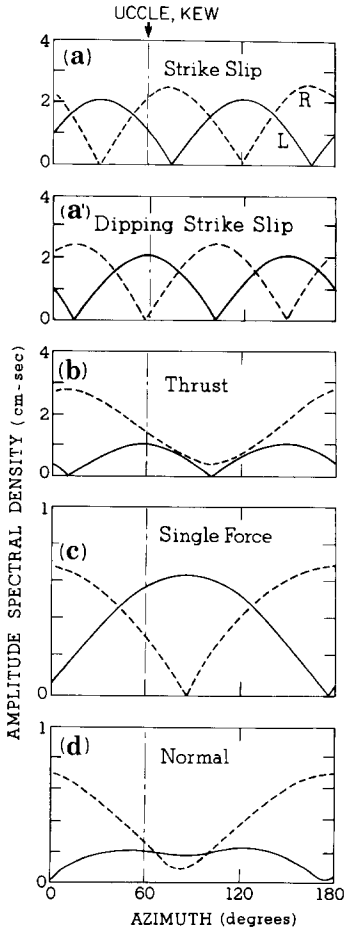

FIG. 5. Amplitude spectrum of surface waves at 50 sec for five mechanisms shown in Figure 2. Solid and dotted curves are for Love waves (transverse component) and Rayleigh (horizontal component) waves, respectively. For double-couple mechanisms, source is step function with seismic moment of 10^{20} dyne-cm. For single-force model, source is step function with force of 10^{20} dynes. Azimuth of stations UCCLE and KEW is indicated by a vertical long-dashed–short-dashed line. Pattern for azimuthal range 180° to 360° is identical to that for 0° and 180° and consequently is omitted.

and the Love- to Rayleigh-wave amplitude ratio (Figure 5a′). However, the direction of the first motion of S wave for this model is toward the south (Table 3), which is inconsistent with the observation.

Thrust mechanism. Since Hasegawa and Herrmann (in preparation) derived a predominantly thrust mechanism (for a focus in the upper mantle) for the M 5.2 earthquake of 1975 that occurred in this area, it is worthwhile to test a comparable thrust mechanism against our data. The P-nodal planes for the corresponding thrust mechanism are shown in Figure 2b, superimposed on our data for the 1929 event. Although these P-nodal planes are inconsistent with the P-wave first motion at two stations, when uncertainties in both the first-motion data and the mechanism are considered, this mechanism is considered acceptable.

However, this thrust mechanism predicts a southward SH first motion at UCCLE and KEW, which is inconsistent with the data (see Table 3). Increasing the dip of the south-dipping plane by about 35° so that the dilatation at La Paz falls in the correct quadrant predicts the same southward SH first motion at UCCLE and KEW.

The surface-wave spectrum computed for this model (Figure 2b) is shown in Figure 5b. At the azimuth of UCCLE and KEW, Rayleigh waves are slightly larger than Love waves for this mechanism, which is inconsistent with the data. A clockwise rotation of the strike of both planes by as much as 60° still predicts a ratio of Rayleigh-to-Love wave that is inconsistent with the data. On the other hand, a counterclockwise rotation of the same amount predicts S-wave polarity that is inconsistent with the data.

Single-force mechanism. A single-force mechanism which represents slumping has only one nearly vertical nodal plane perpendicular to the direction of the maximum slope. Our first-motion data, with the exception of one polarity (at Ann Arbor) that may be questionable, are consistent with this model, as shown in Figure 2c. The compressional hemisphere to the north indicates that the force is directed to the north (upslope direction), which is consistent with the slump model (cf. Kanamori and Given, 1982).

This model predicts northward SH and westward SV with about the same ground amplitude at UCCLE and KEW, which agrees with the observation (Table 3). The data constrict the strike of the nearly vertical (85° dip to north) plane to within a few degrees of the position shown, and consequently no change is predicted for the first motion of SH and SV waves.

The spectral amplitude of Love and Rayleigh waves computed for this model is shown in Figure 5c. At the azimuth of UCCLE and KEW, the model predicts significantly larger Love waves than Rayleigh waves, which is consistent with the observation. A counterclockwise rotation of the force by 20° would increase Love-to-Rayleigh wave amplitude ratio significantly.

Normal-fault mechanism. Eissler and Kanamori (1987) showed that, for the 1975 Kalapana, Hawaii, earthquake, the overall motion can be represented by a single force; however, local first-motion data indicate a normal-fault mechanism (Furumoto and Kovach, 1979). If the slump is initiated at a point embedded in the medium, a normal-fault mechanism is more appropriate to model short-period data.

In view of this result, we test the data for the Grand Banks earthquake using a normal-fault mechanism corresponding to initiation of slumping, as shown in Figure 2d. The P- and S-wave first-motion data are compatible with this mechanism (see Figure 2d and Table 3). However, the surface-wave radiation patterns for this mechanism are inconsistent with the observation, as shown in Figure 5d. The data

constrict the strike and dip of the nearly vertical plane to within a few degrees. Consequently, no change is predicted in the surface-wave radiation pattern.

Summary of the interpretation. The available data are obviously incomplete but, among the possible models considered here, a single-force model is most compatible with the data.

We therefore examine the surface-wave data in further detail using the single-force model in the next section.

SLUMP MODEL

The basic idea of using a single force to model a slump, and formulations for surface-wave excitation by a single force, are described in Kanamori and Given (1982). We will use a slightly modified version of their model. Our model and formulations are described briefly in the Appendix.

We use a horizontal single force which is oriented N5°W, that is upslope in Figure 1. As mentioned previously, the direction of first motion of P and S waves for this mechanism is consistent with our data. Using equation (A1) in the Appendix, we assume a time history of the force given by

$$F_e(t) = \begin{cases} f_0 \sin\left(\dfrac{\pi}{\tau} t\right) & \cdots \quad 0 < t \leqq 2\tau \\ 0 & \qquad\quad t > 2\tau \end{cases} \tag{1}$$

where τ is a constant which determines the time scale of a slump.

The magnitude of the force can be estimated by comparing the observed Love-wave amplitude spectrum with the theoretical excitation computed by equation (A3). Because of the limited bandwidth of the instrument, we use the spectral amplitude only at the 50-sec period.

We first correct the observed spectral amplitude for the instrument, the geometrical spreading, and the attenuation. The gain of the Galitzin instrument at 50 sec is 183 and 69 for UCCLE and KEW, respectively. The combined correction for the geometrical spreading and the attenuation can be calculated from Table 6 of Ben-Menahem *et al.* (1970). The corrected spectral amplitudes are listed in Table 4.

Using (A2) and (A3), the theoretical spectral amplitude for the single force given by (1) can be written as

$$\left| 2\pi f_0 \omega\tau \, \frac{\sin \omega\tau}{\pi^2 - (\omega\tau)^2} \left[-i \, \frac{r_s}{N} \, P_L^{(1)} \cos\delta \sin\phi \right] \right| \tag{2}$$

(for definition of symbols, see the Appendix).

Since we could not determine the spectral shape of the source, it is not possible

TABLE 4

SURFACE-WAVE SPECTRAL DATA AT A 50-SEC PERIOD

Station Component	Trace (cm-sec)	Gain	Ground (cm-sec)	Corrected* (cm-sec)	Theoretical (for 10^{18} dyne)	f_0† (for 10^{20} dyne)
UCCLE T	266	183	1.45	2.9	0.020	1.5
KEW T	85	69	1.24	2.5	0.020	1.3

* Corrected for geometrical spreading and attenuation (Ben-Menahem *et al.*, 1970).

† Peak value of effective force [see equation (A1) or Figure A3c].

to determine τ. For a given ω, equation (2) takes a maximum at $\tau = \pi/\omega = T/2$, where T is the period. Therefore, if $\tau = 25$ sec, surface-wave energy at 50 sec is most efficiently excited. For this value of τ and for a unit force of 10^{18} dynes, the theoretical amplitude is computed and listed in Table 4. Comparing these values with the corrected observed spectral amplitude, we obtain $f_0 = 1.4 \times 10^{20}$ dynes as the average of the values obtained from the two records. If a different value is chosen for τ, a larger value is required for f_0.

These values are comparable with those ($\tau = 90$ sec, $f_0 = 1 \times 10^{20}$ dynes) obtained for the (M_S 7.2) 1975 Kalapana, Hawaii, earthquake (Eissler and Kanamori, 1987). However, because of the incomplete data and of the low gain of the seismographs at long periods, the values obtained for the Grand Banks earthquake are subject to much uncertainty.

In order to check this result, we examined S-wave data. As mentioned earlier, the S wave recorded on the N-S component seismogram of UCCLE is essentially SH. Since body waves are more sensitive to short-period waves, only short-period characteristics of the source can be recovered. We tried to match the observed S-waveform by a synthetic waveform computed for a horizontal single force. The method of calculation is described in Kanamori *et al.* (1984). The time history given by equation (1) yielded a synthetic waveform that has a much longer period than the observed. This is not surprising because the S-waveform is controlled by relatively short-period source characteristics. The source time curve shown in Figure 6c can account for the observed SH waveform (first cycle and one-half) because the associated synthetic waveform in Figure 6b is similar to the observed waveform in Figure 6a. Since the later part of the S-waveform is contaminated by S-coupled PL waves, no effort is made to fit this part. Note the similarity in waveform between the single-force time history shown in Figure 6c with that shown in Figure A3b, where t_1 is the duration of the positive phase (half-cycle) and t_2, the complete cycle (period). In Figure 6, t_1 is about 15 sec, and t_2 is about 50 sec; consequently, the overall period of 50 sec selected for the S-wave single-force time history is comparable to that chosen for the surface-wave analysis. However, the main purpose of this calculation is to see whether the magnitude of the force obtained from surface waves is reasonable or not. By matching the overall amplitude of the SH waves, we

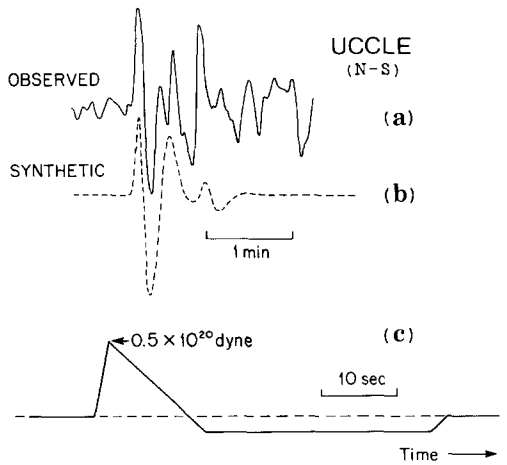

FIG. 6. S wave (N-S component) observed at UCCLE (a) and synthetic S wave computed for single force (b), with corresponding source time history shown at *bottom* (c). Net impulse for this force is zero.

calculated the peak value of the force-time function (f_0) to be 0.5×10^{20} dynes, which is somewhat smaller than that computed from surface waves. However, since the S wave represents a relatively short-period part of the source, the agreement between these values is considered good. This good agreement suggests that $f_0 = 1.4 \times 10^{20}$ dynes obtained from surface waves is reasonable.

From the magnitude of the force thus estimated from surface-wave data (and substantiated by SH-wave synthesis), the volume of sediments associated with this submarine landslide can be estimated in the following manner. The mean force, $F_s (F_s \simeq \frac{1}{2} f_0)$ is related to the volume by $F_s = V\rho\, g \sin A$, where V is volume, ρ is effective density (actual density minus density of water), g is the acceleration due to gravity, and A is the average inclination of the continental slope in the epicentral area. For $F_s = 7 \times 10^{19}$ dynes, $\rho = 1.5$ gm/cm^3 and $A = 5°$ (see Piper *et al.*, 1985a), $V = 5.5 \times 10^{11}$ m^3. The areal extent of the slump, as based on a seismic reflection profile and core samples (Heezen and Drake, 1964), is shown in Figure 7. The area of "instantaneous" cable break (Piper *et al.*, 1985a) is shown in Figure 8. The remarkable coincidence between these two areas indicates a major sediment slide block with lateral dimensions of approximately 250 km by 150 km, or an area of 37,500 km^2. A seismic reflection profile along the dotted line segment in Figure 7 (Heezen and Drake, 1964) also indicates a continuous depression in the sediments along the continental slope, commencing near the epicenter and extending downslope about 110 km. On the basis of the slide area previously quoted and our

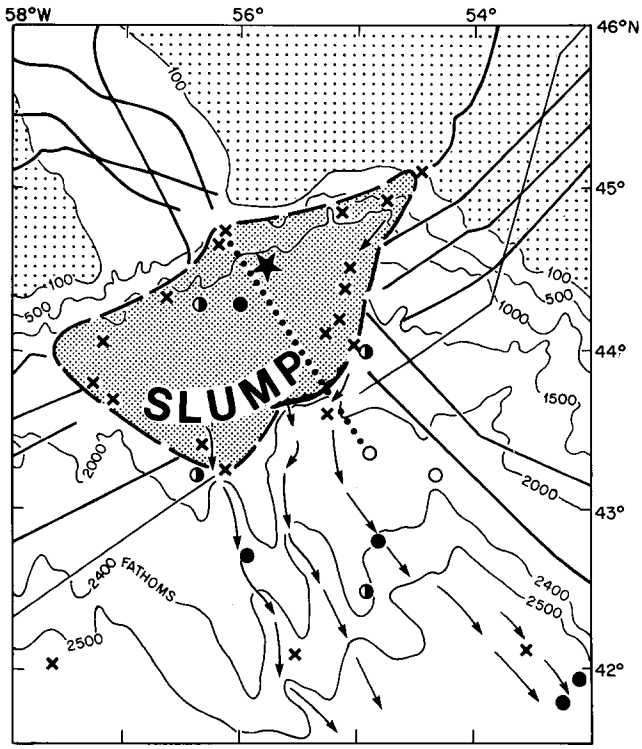

FIG. 7. Epicenter of 1929 earthquake (star) shown in relation to slump area (outcrop of sole of slump shown as solid arc), cables (solid lines), cable breaks (crosses), and core samples (solid dot denotes sands and silts; half-filled circles denote disturbed hemipelagic sediments; open circles denote undisturbed hemipelagic sediments). Bathymetry contours are in fathoms (1 fathom = 1.8 m). Dotted line represents seismic reflection profile. Arrows represent direction of turbidity current (from Heezen and Drake, 1964).

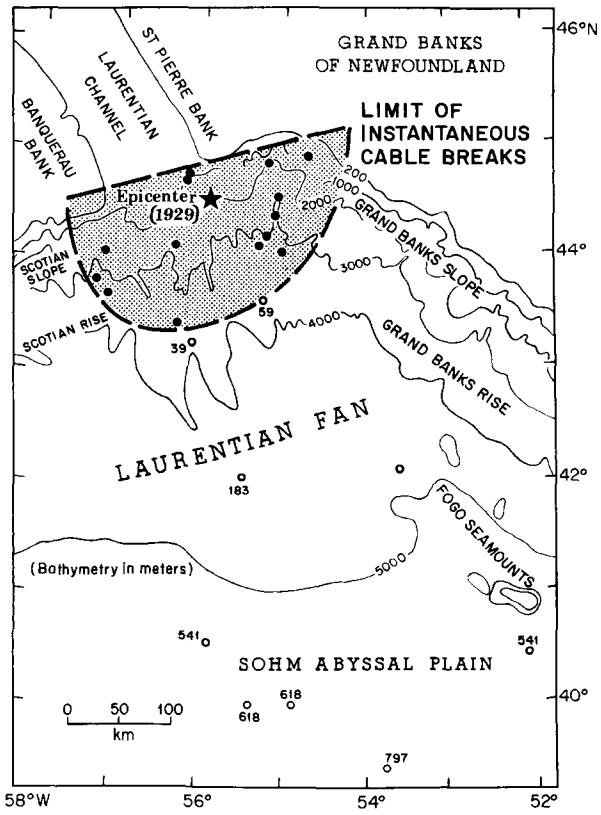

FIG. 8. Epicenter of 1929 earthquake (star) shown in relation to locations of "instantaneous" cable breaks, which are represented by solid dots, and locations of succeeding cable breaks, which are shown by open circles with time (minutes) after onset of slumping (from Piper and Normark, 1982). Dashed lines encompass area of "instantaneous" cable breaks (from Piper *et al.*, 1985a). Slumping was probably initiated near the epicenter (star) and propagated outward (laterally and downslope).

calculation of slide volume of 5.5×10^{11} m^3, the average thickness of the slide material is 15 m. Even though accurate estimates of the sediment slide volume of the 1929 event are intrinsically difficult to measure, due in part to considerable lateral variation in the apparent thickness of the slide material, direct measurements of at least 1×10^{11} m^3 (by Piper and Aksu, 1987) are in agreement (within a factor of five) with our calculations based on both surface- and body-wave analyses. If the seismic reflection profile down the Laurentian slope is applicable over the entire slump area, then our estimate of slump volume of 5×10^{11} m^3 is compatible with their (Heezen and Drake, 1964) profile.

The close agreement between estimates of sediment slide volume based on a single force with that based on *in situ* measurements is an argument in favor of the view that a significant portion of the teleseismic surface- and body-wave signals (especially at KEW and UCCLE) were generated by a submarine sediment slide. However, because of the limited seismic data, it is also possible that a (double-couple) earthquake generated much of the observed teleseismic signals. But, whatever the seismic event may be, it must satisfy the *P*-, *S*-, and surface-wave data presented in this paper.

Potential trigger mechanisms for this submarine sediment slide are (internal) precursory small landslides or (external) strong ground vibrations from a nearby

moderate earthquake. *P*-wave signatures of the 1929 event are generally small (less than several millimeters peak-to-peak) and extremely irregular and complex (even on KEW and UCCLE records). In addition, it is inherently difficult to differentiate between *P*-wave signals from precursory landslides and earthquakes. Thus, from an inspection of *P*-wave records, we were not able to determine which of the two possible trigger mechanisms is the more likely one. A moderate earthquake at the epicenter shown for the 1929 event could have generated strong ground vibrations that initiated submarine sediment sliding at the epicenter, with the area of sliding expanding rapidly laterally along the continental margin and down the continental slope to a radial distance slightly in excess of 100 km. The semi-circular area of radius slightly greater than 100 km coincides with the region where the sediments on the slope were in unstable equilibrium. If liquefaction was required to initiate slumping, then the size of the trigger earthquake would have to be about magnitude 6 (e.g., see Atkinson *et al.*, 1984); however, if only strong ground motion (without liquefaction) is sufficient, then the size of the earthquake required to initiate slumping could be much less than magnitude 6.

Although details of many of the sediment slide areas along the continental slope are described in several papers (e.g., Piper and Normark, 1982; Piper *et al.*, 1985a, b; Piper and Aksu, 1987; Piper *et al.*, 1987), the mechanism and the spatiotemporal history of the complex sediment slide sequence for the 1929 event are not properly understood. Thus, the possibility of an internal trigger mechanism for the sediment slide cannot be ruled out.

We note a remarkable similarity between the Grand Banks earthquake and the Kalapana earthquake. The surface-wave magnitude (7.2), the long-period spectral amplitude, and the geometrical relation between the *P*-wave mechanism diagram and the maximum slope direction are all similar between the two events. For the Kalapana earthquake, Eissler and Kanamori (1987) demonstrated that the seismic observations can be explained most reasonably by a large scale slumping. In view of this similarity, we feel that the slump mechanism for the Grand Banks earthquake is a distinct possibility, even though there is an apparently slight discrepancy between the various estimates of the volume of sediment sliding. Because the actual spatiotemporal history of sediment sliding over the entire slump area is likely to be extremely complex (A. Ruffman, personal communication, 1987) and therefore inherently difficult to model with any degree of confidence, the consequence of including this finiteness-of-source effect on estimates of f_0 [see equation (1)] is uncertain and beyond the scope of this study.

Estimates of maximum tsunami heights along the southern coast of Newfoundland (north of the epicenter) vary considerably, but tend to fall in the range of 4 to 12 m (McIntosh, 1930; Johnstone, 1930; Murty and Wigen, 1976). In contrast, tsunami heights were about an order-of-magnitude smaller to the west along the coastline of Nova Scotia (see Murty and Wigen, 1976). This tsunami radiation pattern is likely due to a combination of the direction of submarine slumping and nature of seafloor relief between source and coastline. The arrival of the tsunami along coastal regions north and west of the epicenter coincided with high tide.

Discussion

Seismic data that we have been able to collect for the 1929 event are in agreement with a single-force source mechanism. The double-couple models proposed so far are not consistent with the *S*-wave and surface-wave data. This does not mean,

however, that our data preclude alternate double-couple models. It may be possible to find some double-couple models that satisfy the *P*-, *S*-, and surface-wave data.

Sudden slumping of a large mass of sedimentary deposits on the continental slope can modify the horizontal (deviatoric) stress field to depths of 40 km or more and thereby trigger "aftershocks." Hasegawa *et al.* (1979) showed how sedimentary deposits along a passive continental margin generate horizontal (deviatoric) extension under the load to depths of 40 km or more. Therefore, sedimentary unloading (as a consequence of slumping) would generate the opposite effect, namely horizontal (deviatoric) compression in this depth range. Analysis of the magnitude 5.2 Laurentian Channel earthquake indicates a 30 km focal depth and a subhorizontal deviatoric compression vector. Thus, large-scale sedimentary slumping can affect, indirectly, the seismic activity (see Figure 1) along the continental margin by modifying the ambient stress field. Faults parallel to the Scotian shelf (e.g., see Turcotte *et al.*, 1977) or parallel to the trend of the Laurentian Channel (see King and Maclean, 1976; King, 1980) would be most susceptible to failure under the modified stress field.

There are two viewpoints with respect to the manner and rate of sediment buildup along the continental slope of eastern Canada. One view is that the sedimentation rate on the continental slope at the mouth of the Laurentian Channel is governed by the rate of flow of sediments down the Laurentian Channel. On the basis of sedimentation rate data (for summary, see Piper and Normark, 1982), at least 100,000 yr is required to replenish the volume of sediments displaced by the 1929 event. For this case, the return period of a tsunamigenic event of $M \sim 7$ is at least 100,000 yr, and epicenters would be confined to the mouth of the Laurentian Channel, since the St. Laurence River is the biggest depositor of sediments along the southeast coast of Canada. A more recent view (see Piper *et al.*, 1985a) is that sediments along the continental slope may be deposited mainly by glaciers, and sediments such as those deposited at the mouth of the Laurentian Channel may be common along the entire continental slope of eastern Canada. For this case, at any specified site along the continental slope, the return period of an $M \sim 7$ event would be about 20,000 yr, which is the approximate return period of miniglaciers (see Bloom *et al.*, 1974), given that the slump is the only causative mechanism for large earthquakes; tsunamigenic events would be possible, not only at the mouth of the Laurentian Channel, but also possibly along the entire coast line. These two cases imply that the trigger mechanism or cause of larger seismic events along the continental slope, whether the source mechanism be rupture along a weakened zone or fault at shallow (~10 to ~20 km) depths (e.g., see Turcotte *et al.*, 1977) or a submarine (sedimentary) landslide, is governed more by the rate and nature of sedimentation along the slope rather than by neotectonic forces such as spreading ridge stress.

The other possibility is that large seismic events along the continental margin may be influenced more by neotectonic stresses such as spreading ridge stress (see Hasegawa *et al.*, 1985) and stresses induced by continent-to-ocean transition zone (e.g., see Bott and Dean, 1972) rather than to stresses related to sedimentary loading or slumping. For this case, large earthquakes would occur more frequently in regions where there is more rapid buildup of neotectonic forces, especially in regions where there are weakened zones such as unhealed ruptures from previous large earthquakes or from the last major tectonic orogeny. On the basis of cumulative magnitude-recurrence relations for Laurentian slope earthquakes, and assumption that future

seismic activity will be similar to the past, the return period of a tectonic earthquake of magnitude 7 varies from 300 to 1,000 yr; an alternate hypothesis is that a tectonic earthquake of this magnitude could occur randomly anywhere along the continental margin, and, for this case, the return period along any 100 km segment is of the order of 5,000 to 10,000 yr (see Basham *et al.*, 1983). Thus, with respect to hydrocarbon exploration in this region, the seismic hazard is greater for this case than for the case of sediment sliding, which has a much longer return period. The effect of sediment loading-unloading on the repeat time of tectonic, thrust-fault earthquakes would vary, depending on the phase of the sediment load-unload cycle. Consider the neutral stress state with respect to sediment loading-unloading to be mid-way between successive slump episodes. During the loading phase, deviatoric horizontal extension at depth would increase monotonically and thereby lengthen the repeat time of tectonic, thrust-fault earthquakes. Then, immediately after a major slump, deviatoric horizontal compression would be at a maximum and gradually decrease to zero mid-way between the major slumps. The return period of thrust-fault earthquakes would be at a minimum just after the slump (cf. Smith, 1966) and gradually increase to that for the ambient tectonic return cycle. The aforementioned argument only pertains to a predominantly thrust-fault type of seismotectonic stress regime.

ACKNOWLEDGMENTS

We thank the many institutions that sent us requested copies of seismograms of this noteworthy historical earthquake. Comments on various aspects of this paper by the following are appreciated: J. Adams; R. J. Wetmiller; M. J. Berry; P. W. Basham; H. Eissler; and the reviewers. We thank D. J. W. Piper for sending us preprints of two of his papers. Discussions with A. Ruffman on complexities of sediment slumping were helpful.

This work was partially supported by the National Science Foundation Grant ECE-8303647.

REFERENCES

Ando, M. (1979). The Hawaii earthquake of November 29, 1975: low dip angle faulting due to forceful injection of magma, *J. Geophys. Res.* **84,** 7616–7626.

Atkinson, G. M., W. D. Liam Finn, and R. G. Charlwood (1984). Simple computation of liquefaction probability for seismic hazard applications, *Earthquake Spectra* **1,** 107–123.

Basham, P. W., J. Adams, and F. M. Anglin (1983). Earthquake source models for estimating seismic risk on the eastern Canadian continental margin, in *Proceedings of the Fourth Canadian Conference on Earthquake Engineering*, Vancouver, Canada, June 15–17, 1983, 495–508.

Ben-Menahem, A., M. Rosenman, and D. G. Harkrider (1970). Fast evaluation of source parameters from isolated surface-wave signals, *Bull. Seism. Soc. Am.* **60,** 1337–1387.

Bloom, A. L., W. S. Broecker, J. M. A. Chappel, R. K. Mathews, and K. J. Mesolella (1974). Quaternary sea level fluctuations on a tectonic coast: new $^{230}TH/^{234}U$ dates from the Huon Peninsula, New Guinea, *Quat. Res.* **4,** 185–205.

Bott, M. H. P. and D. S. Dean (1972). Stress systems at young continental margins, *Nature Phys. Sci.* **235,** 23–25.

Crosson, R. S. and E. T. Endo (1981). Focal mechanisms of earthquakes related to the 29 November 1975 Kalapana, Hawaii, earthquake: the effect of structure models, *Bull. Seism. Soc. Am.* **71,** 713–729.

Crosson, R. S. and E. T. Endo (1982). Focal mechanisms and locations of earthquakes in the vicinity of the 1975 Kalapana earthquake aftershock zone, 1970–1979: implications for tectonics of the south flank of Kilauea Volcano, Island of Hawaii, *Tectonics* **1,** 495–542.

Dewey, J. W. and D. W. Gordon (1984). Map showing recomputed hypocenters of earthquakes in the eastern and central United States and adjacent Canada, 1925–1980, Department of the Interior, U.S. Geological Survey, Miscellaneous Field Studies, Map MF-1699, 13.

Doxsee, W. W. (1948). The Grand Banks earthquake of November 18, 1929, *Publ. Dom. Observ.* **7,** 323–335.

Eissler, H. K. and H. Kanamori (1987). A single-force model for the 1975 Kalapana, Hawaii, earthquake, *J. Geophys. Res.* **92,** 4827–4836.

Fletcher, J. B., M. L. Sbar, and L. R. Sykes (1978). Seismic trends and travel-time residuals in eastern North America and their tectonic implications, *Geol. Soc. Am. Bull.* **89,** 1656–1676.

Furumoto, A. S. and R. L. Kovach (1979). The Kalapana earthquake of November 29, 1975: an intraplate earthquake and its relation to geothermal processes, *Phys. Earth Planet. Interiors* **18,** 197–208.

Glover, D. P. and H. Meyers (1982). Historical seismogram filming project: fourth progress report, SE-33, World Data Center A for Solid Earth Geophysics, Boulder, Colorado, 54 pp.

Gussow, W. C. (1982). The Grand Bank earthquake of 1929. *Discussions in Geosci. Can.* **9,** 122–123.

Gutenberg, B. and C. F. Richter (1956). Magnitude and energy of earthquakes, *Ann. Geofis.* **9,** 1–15.

Hasegawa, H. S., C. W. Chou, and P. W. Basham (1979). Seismotectonics of the Beaufort Sea, *Can J. Earth Sci.* **16,** 816–830.

Hasegawa, H. S., J. Adams, and K. Yamazaki (1985). Upper crustal stresses and vertical stress migration in eastern Canada, *J. Geophys. Res.* **90,** 3637–3648.

Heezen, B. C. and C. L. Drake (1964). Grand Banks slump, *Bull. Am. Assoc. Petrol. Geologists* **48,** 221–233.

Heezen, B. C. and M. Ewing (1952). Turbidity currents and submarine slumps, and the 1929 Grand Banks earthquake, *Am. J. Sci.* **250,** 849–873.

Johnstone, J. H. L. (1930). The Acadian-Newfoundland earthquake of November 18, 1929, *Trans. Nova Scotian Inst. Sci.* **XVII,** 223–237.

Kanamori, H. (1972). Mechanism of tsunami earthquakes, *Phys. Earth Planet. Interiors* **6,** 346–359.

Kanamori, H. (1985). Non-double couple seismic source (abstract), The 23rd General Assembly of International Association of Seismology and Physics of the Earth's Interior, Tokyo, Japan, August 19–30, 425.

Kanamori, H. and J. W. Given (1982). Analysis of long-period seismic waves excited by the May 18, 1980, eruption of Mount St. Helens—A terrestrial monopole? *J. Geophys. Res.* **87,** 5422–5432.

Kanamori, H., J. W. Given, and T. Lay (1984). Analysis of seismic body waves excited by the Mount St. Helens eruption of May 18, 1980, *J. Geophys. Res.* **89,** 1856–1866.

King, L. H. (1980). Aspects of regional surficial geology related to site investigation requirements—Eastern Canadian shelf, in *Offshore Site Investigations*, D. A. Ardus, Editor, Graham and Trotman, London, England, 37–57.

King, L. H. and B. Maclean (1976). Geology of the Scotian Shelf, *Geol. Surv. Can. Paper 74-31*, 31 pp.

McIntosh, D. S. (1930). The Acadian-Newfoundland earthquake, *Trans. Nova Scotian Inst. Sci.* **XVII,** 213–222.

Murty, T. S. and S. O. Wigen (1976). Tsunami behaviour on the Atlantic coast of Canada and some similarities to the Peru coast, *R. Soc. New Zealand Bull.* **15,** 51–60.

Nakamura, K. (1980). Why do long rift zones develop in Hawaiian volcanoes (in Japanese), *Kazan* **25,** 255–269.

Page, R. A. and P. W. Basham (1985). Earthquake hazards in the offshore environment, *U.S. Geol. Surv. Bull. 1630*, 69 pp.

Piper, D. J. W. and W. R. Normark (1982). Effects of the 1929 Grand Banks earthquake on the continental slope off eastern Canada, in *Current Research*, Part B, *Geol. Surv. Can. Paper 82-1B*, 147–151.

Piper, D. J. W. and A. E. Aksu (1987). The source and origin of the 1929 Grand Banks turbidity current inferred from sediment budgets, *Geo-marine Letters* (in press).

Piper, D. J. W., R. Sparkes, D. C. Mosher, A. N. Shor, and J. A. Farre (1985a). Seabed instability near the epicentre of the 1929 Grand Banks earthquake, *Geol. Surv. Can. Open-File Rept. 1131*, 55 pp.

Piper, D. J. W., A. N. Shor, J. A. Farre, S. O'Connell, and R. Jacobi (1985b). Sediment slides and turbidity currents on the Laurentian Fan: sidescan sonar investigations near the epicenter of the 1929 Grand Banks earthquake, *Geology* **13,** 538–541.

Piper, D. J. W., A. N. Shor, and J. E. H. Clarke (1987). The 1929 Grand Banks earthquake, slump and turbidity current, *Geol. Soc. Am. Special Paper* (in press).

Podrouzek, A. J. and J. S. Bell (1985). Stress orientations from wellbore breakouts on the Scotian Shelf, Eastern Canada, in *Current Research*, Part B, *Geol. Surv. Can. Paper 85-1B*, 59–62.

Smith, W. E. T. (1966). Earthquakes of eastern Canada and adjacent areas 1928–1959, *Publ. Dom. Observ.* **XXXII,** 87–121.

Stewart, G. S. (1979). The Grand Banks earthquake of November 18, 1929 and the Bermuda earthquake of March 24, 1978–A comparative study in relation to their intraplate location (abstract), *EOS* **60,** 312.

Turcotte, D. L., J. L. Ahern, and J. M. Bird (1977). The state of stress at continental margins, *Tectonophysics* **42**, 1–23.

GEOPHYSICS DIVISION
GEOLOGICAL SURVEY OF CANADA
OTTAWA, ONTARIO K1A 0Y3, CANADA (H.S.H.)
CONTRIBUTION NO. 21786

DIVISION OF GEOLOGICAL AND
PLANETARY SCIENCES
SEISMOLOGICAL LABORATORY
CALIFORNIA INSTITUTE OF TECHNOLOGY
PASADENA, CALIFORNIA 91125 (H.K.)
CONTRIBUTION NO. 4456

Manuscript received 25 June 1986

APPENDIX

The spatiotemporal pattern of "instantaneous" submarine slumping is quite complex (see Piper and Normark, 1982; Piper *et al.*, 1985a). In addition, the actual physical mechanisms for initiation and termination, especially the latter, of slumping are not fully understood. Therefore, we have selected a simple model to represent this rather complex phenomenon. The selected model consists of a block on an incline of constant slope with variations in sliding (Coulomb) friction to initiate and terminate slumping.

Figure A1 shows four stages in the cycle of unstable sediments sliding down the continental slope. In Figure A1a, the sedimentary block is at rest and F_s the interaction force parallel to slope, is $F_s = Mg \sin A$, where M is the mass of the sediments, g is the acceleration due to gravity, and A is the average inclination of the continental slope. At time $t = 0$ (Figure A1b), instability occurs, and the block

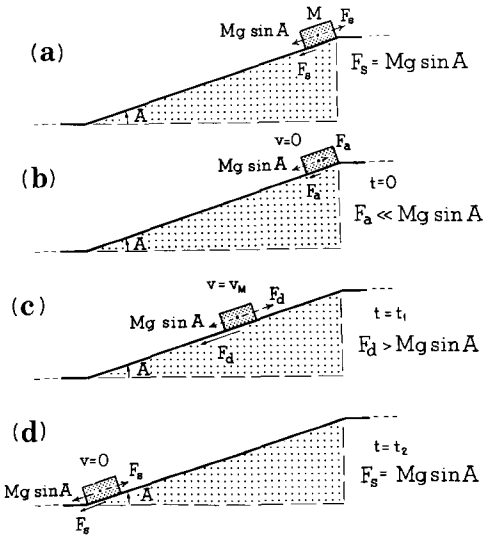

FIG. A1. Simplified model of (sedimentary) block sliding down incline (continental slope) and associated interaction forces (parallel to slope). Solid arrows represent forces acting on continental slope, whereas dashed arrows represent forces acting on overlying block. In (a), block (effective mass M) is at rest and static frictional force (F_s) equals the pull of gravity (Mg sin A), where g is acceleration due to gravity. In (b), at time $t = 0$, block starts to slide (accelerate) as dynamic frictional stress (F_a) is much less than gravitational pull. In (c), at time $t = t_1$, maximum velocity $V = V_m$ is attained, and block starts to decelerate as frictional force F_d becomes greater than the gravitational pull. In (d), block comes to rest at $t = t_2$.

begins to slide. The force of interaction during the acceleration stage, F_a, is much less than F_s because sliding friction (F_a) is generally much less than static friction (F_s). At $t = t_1$ (Figure A1c), the deceleration stage commences and the force of interaction, F_d, becomes greater than F_s and the block comes to rest at $t = t_2$ (Figure A1d).

Figure A2 is a simplified version of the actual time history of the force exerted by the block on the underlying slope as it slides down the slope. Figure A3 shows the time history of the "effective" force, i.e., the force-time history related to seismic wave generation. [The initial (zero) level corresponds to the F_s level in Figure A2.] During the acceleration stage, the effective force is in the upslope direction, and during the deceleration stage, in the downslope direction. A physically more realistic time history of the effective force is shown in Figure A3b. A necessary constraint on the time history is that the area above the time (t) axis equals that below this axis; i.e., the total impulse must be zero. In order to facilitate subsequent calculations

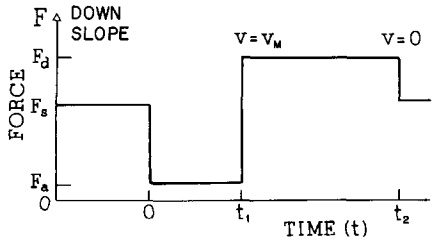

FIG. A2. Temporal behavior of interaction forces on continental slope. F_s is static frictional force, F_a is force during acceleration stage (time $t = 0$ to t_1), and F_d is force during deceleration stage (t_1 to t_2) (see Figure A1). Other symbols are as defined in Figure A1.

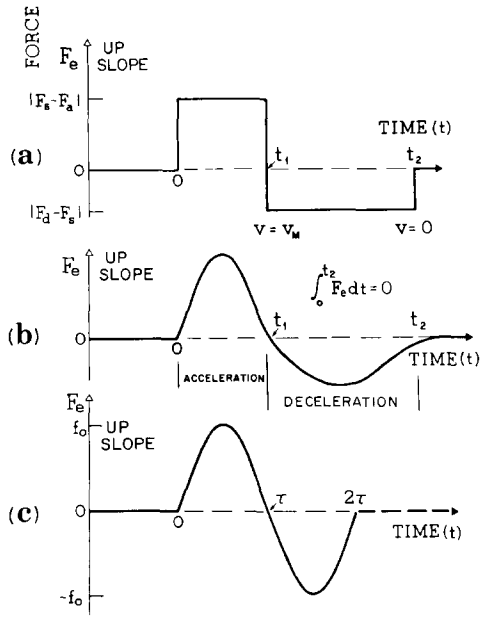

FIG. A3. Effective force (F_e) acting on continental slope is related to seismic energy generation. Equilibrium condition prevails before $t = 0$, i.e., $F_e = 0$, as no seismic energy is generated. In (a), from $t = 0$ to $t = t_1$, slope experiences effective force upslope as $F_a \leqq F_s$. From $t = t_1$ to $t = t_2$, slope experiences effective force downslope. In (b), physically more realistic temporal behavior of effective force is shown. In (c), temporal pattern of effective force shown in (b) is modified slightly and replaced with sinusoidal force (of period 2τ and peak amplitude f_0) for mathematical tractability [see equation (A1)].

of source characteristics, a simple sinusoidal source-time function, as shown in Figure A3c, is chosen to simulate the effective force function, F_e, which is

$$F_e(t) = f_0 \sin\left(\frac{\pi}{\tau} t\right) \cdots \tag{A1}$$

where f_0 is the peak value and 2τ, the period. The Fourier transform of $F_e(t)$ is

$$\hat{F}_e(\omega) = 2\pi f_0 \tau i \frac{\sin(\omega\tau)}{\pi^2 - (\omega\tau)^2} e^{-i\omega\tau} \cdots \tag{A2}$$

where ω is angular frequency, 2τ is the period, and the other symbols are as described previously.

The asymptotic (far-field) form for surface-wave ground displacement (U) due to a single force is (Kanamori and Given, 1982)

$$U_\phi{}^L(\theta, t) = \frac{1}{2\pi} \int_{-\infty}^{+\infty} C_L(\omega) e^{i\omega t}\, d\omega,$$

where

$$C_L(\omega) = \frac{1}{\sqrt{\sin\theta}} \cdot \exp\left(-\frac{1}{4}\pi i\right) \cdot \exp(-i\omega a\theta/C) \cdot \left[-i \frac{r_s}{N} P_L{}^{(1)} \cos\delta \cdot \sin\phi\right] \cdots \tag{A3}$$

and

$$U_r{}^R(\theta, t) = \frac{1}{2\pi} \int_{-\infty}^{+\infty} C_R(\omega) e^{i\omega t}\, d\omega,$$

where

$$C_R(\omega) = \frac{1}{\sqrt{\sin\theta}} \cdot \exp\left(+\frac{1}{4}\pi i\right) \cdot \exp(-i\omega a\theta/C) \cdot \left[\frac{r_s P_R{}^{(1)}}{N} \cdot \left\{\frac{\sin\delta}{N} \cdot \frac{Y_1(r_s)}{Y_3(r_s)} + i\cos\delta \cdot \cos\phi\right\}\right]. \tag{A4}$$

In equations (A3) and (A4), $U_\phi{}^L$ and $U_r{}^R$ represent the transverse horizontal (Love) and radial (Rayleigh horizontal) components respectively, θ is angular distance from source to receiver, t is time, a is radius of Earth, r_s is distance from the center of the Earth to earthquake focus, C is phase velocity, N is order number of mode having angular frequency ω, δ is plunge of single force, ϕ (right of equal sign) is azimuth of the station measured counterclockwise from the horizontal projection of force [$F_e(t)$ in equation (A1)]. $P_L{}^{(1)}$ and $P_R{}^{(1)}$ are the excitation functions for

Rayleigh and Love waves (as tabulated by Kanamori and Given, 1982). The term $\frac{Y_1(r_s)}{NY_3(r_s)}$ is approximately -1.5 at the surface for the fundamental Rayleigh mode. Equations (A3) and (A4) are for a force for which the time function is a unit step function; consequently, the sinusoidal force function, $\hat{F}_e(\omega)$ of equation (A2) must be multiplied by $i\omega$ when equation (A2) is used in conjunction with equations (A3) and (A4).